Electronic Influences on Metallophilic Interactions in $[Pt(tpy)X][Au(C_6F_5)_2]$ Double Salts

Val Phillips,[†] Kathryn J. Willard,[‡] James A. Golen,[§,∥] Curtis J. Moore,[§] Arnold L. Rheingold,[§] and Linda H. Doerrer*[,†]

[†]*Chemistry Department, Boston University, 590 Commonwealth Avenue, Boston, Massachusetts 02215,* [‡]*Chemistry Department, Barnard College, 3009 Broadway, New York, New York 10027,* [§]*Department of Chemistry and Biochemistry, University of California, San Diego, 9500 Gilman Drive, La Jolla, California 92093-0358, and* [∥]*Department of Chemistry & Biochemistry, University of Massachusetts Dartmouth, North Dartmouth, Massachusetts 02747*

Four double salt compounds of the type $[Pt(tpy)X][Au(C_6F_5)_2]$, where tpy =2,2′:6′,2″-terpyridine and X = Cl, **3**, Br, **4**, I, **5**, and CCPh, **6**, and their platinum starting materials, $[Pt(tpy)Br]Br \cdot 2H_2O$, **1**, and $[Pt(tpy)(CCPh)]PF_6 \cdot DMF \cdot H_2O$, **2**, have been synthesized and characterized. Complex **2** is a solvated form of the known and structurally characterized $[Pt(tpy)(CCPh)]PF_6$ species. All compounds were characterized by single-crystal X-ray diffraction, elemental analyses, and solution electronic spectra. Structural characterization shows that compounds **3** and **4** are similar in the solid state and form cation−anion stacking patterns while compounds **5** and **6** form chains of cations supported by metallophilic interactions with anion partners on either side of the chains. Solution studies (UV−vis and fluorescence) strongly suggest that there are no Pt···Au interactions in solution state. Electronic structure calculations with density functional theory (DFT) elucidate the subtle changes in the electronic scaffolding of the ions in these compounds and show that predictions of metallophilic interactions are not straightforward but can be understood in terms of orbital symmetry and the relative energies of the frontier orbitals.

Introduction

Since its initial empirical observation with gold in the dication $[(Ph_3PAu)_6C]^{2+}$,[1,2] metallophilicity[3] has been observed in many other metal complexes having two or more metals associated via either closed-shell (e.g., $d^{10}···d^{10}$),[4,5] pseudo-closed-shell ($d^8···d^8$),[6] or mixed ($d^8···d^{10}$)[7−12] electronic configurations. A survey of the literature reveals a wealth of examples displaying metallophilicity in homometallic systems such as $Au^I···Au^I$ interactions[4,5] or $Pt^{II}···Pt^{II}$ combinations[6] and few examples of interactions between mixed metal, heterometallic derivatives such as $Pt^{II}···Au^I$,[7] $Au^I···Ag^I$,[13] and $Au^I···Tl^I$ pairings.[14] Among these examples of mixed metal systems is our work with $Pt^{II}···Au^I$ double salt complexes of the form $[M]^+[M']^-$ composed of heavy metal containing cations and anions.[7,15−17] These double salts were developed in a bottom-up approach to atomically thin one-dimensional (1D) arrays of metal atoms. Such highly anisotropic structures have been of interest for many years as potentially electronically conducting materials.[18] Essential for electron transport through a chain

*To whom correspondence should be addressed. E-mail: doerrer@bu.edu.

(1) Scherbaum, F.; Grohmann, A.; Huber, B.; Krueger, C.; Schmidbaur, H. *Angew. Chem., Int. Ed. Engl.* **1988**, *27*, 1544.
(2) Schmidbaur, H.; Schier, A. *Chem. Soc. Rev.* **2008**, *37*, 1931.
(3) Pyykkö, P. *Chem. Rev.* **1997**, *97*, 597.
(4) Yam, V. W.-W.; Lo, K. K.-W. *Chem. Soc. Rev.* **1999**, *28*, 323.
(5) Che, C.-M.; Lai, S.-W. *Coord. Chem. Rev.* **2005**, *249*, 1296.
(6) Angle, C. S.; DiPasquale, A. G.; Rheingold, A. L.; Doerrer, L. H. *Acta Crystallogr., Sect. C: Cryst. Struct. Commun.* **2006**, *C62*, m340.
(7) Doerrer, L. H. *Comments Inorg. Chem.* **2008**, *29*, 93.
(8) Kim, M.; Taylor, T. J.; Gabbai, F. P. *J. Am. Chem. Soc.* **2008**, *130*, 6332.
(9) Fernandez, E. J.; Laguna, A.; Lopez-de-Luzuriaga, J. M.; Monge, M.; Nema, M.; Olmos, M. E.; Perez, J.; Silvestru, C. *Chem. Commun.* **2007**, 571.
(10) Chen, W.; Liu, F.; Xu, D.; Matsumoto, K.; Kishi, S.; Kato, M. *Inorg. Chem.* **2006**, *45*, 5552.
(11) Stork, J. R.; Rios, D.; Pham, D.; Bicocca, V.; Olmstead, M. M.; Balch, A. L. *Inorg. Chem.* **2005**, *44*, 3466.
(12) Uson, R.; Fornies, J.; Falvello, L. R.; Uson, M. A.; Uson, I. *Inorg. Chem.* **1992**, *31*, 3697.
(13) Schuster, O.; Monkowius, U.; Schmidbaur, H.; Ray, R. S.; Krueger, S.; Roesch, N. *Organometallics* **2006**, *25*, 1004.
(14) Crespo, O.; Laguna, A.; Fernandez, E. J.; Lopez-de-Luzuriaga, J. M.; Mendia, A.; Monge, M.; Olmos, E.; Jones, P. G. *Chem. Commun.* **1998**, 2233.
(15) Angle, C. S.; Woolard, K. J.; Kahn, M. I.; Golen, J. A.; Rheingold, A. L.; Doerrer, L. H. *Acta Crystallogr., Sect. C: Cryst. Struct. Commun.* **2007**, *C63*, m231.
(16) Kahn, M. I.; Golen, J. A.; Rheingold, A. L.; Doerrer, L. H. *Acta Crystallogr., Sect. E: Struct. Rep. Online* **2009**, *E65*, m1135/1.
(17) Doerrer, L. H. *Dalton Trans.* **2010**, *39*, 3543.
(18) *Extended Linear Chain Compounds*; Miller, J. S., Ed.; Plenum Press: New York, 1982.

of metal atoms is close contact between each neighboring pair of metal ions. To facilitate close metal−metal contacts, we imposed the following guidelines on our double salts: (1) both cation and anion must contain metals with either closed-shell or pseudo-closed-shell electronic configurations that favor metallophilic interactions, (2) both cation and anion must have linear or square planar geometry to minimize steric hindrance, and (3) both cation and anion must be singly charged for solubility purposes.[15,16,19] A more detailed discussion of these systems can be found in a recent review.[7]

Using these guidelines, our laboratory has been successful in synthesizing and characterizing a large family of double salt complexes of the forms $[Pt^{II}L_3X][Au^IX_2]$, $[Pt^{II}L_3X]$-$[Au^{III}X_4]$, $[Au^{III}L_2X_2][Au^IX_2]$, and $[Au^{III}L_2X_2][Au^{III}X_4]$ where L_2 and L_3 are neutral bidentate or tridentate planar ligands, respectively, and X is either a halogen or a pseudo-halogen.[7] The $[PtL_3X][AuX_2]$ family is by far the most developed, with most examples involving the well studied $[Pt(tpy)Cl]^+$ moiety.[19] Structural characterization of some of these complexes has revealed metallophilic interactions between pairs of $Pt^{II}\cdots Pt^{II}$ cations[15] and metallophilic interactions between $Pt^{II}\cdots Au^I$,[19] and $Au^{III}\cdots Au^{III}$ species[19] that can form infinite chains of contacts. This bottom-up preparation of metallophilic chains has demonstrated the feasibility of our double salt approach and laid the foundations for two new modifications of these systems. First, the low solubility of some complexes led to difficulties in recrystallization such that with added heat, undesired X-type ligand scrambling between the Pt^{II} and Au^I ions and partial reduction of some Au^{III} anions to Au^I anions was observed.[19] Therefore, we sought alternative ligand derivatives that would improve solubility and eliminate ligand scrambling and reduction behaviors. We have chosen to increase the solubility and substitutional robustness of the $[AuX_2]^-$ component by using the $[Au(C_6F_5)_2]^-$ anion developed by Uson et al.[20,21] and used extensively by the Laguna group.[22] Both the robustness of this molecule and its ability to form metal−metal interactions with both Ag^I and Tl^I metal centers has been demonstrated in numerous reports.[14,23−25] Additionally, the π-conjugated X group was proposed to facilitate π-interactions with the tpy ligand of the $[Pt(tpy)X]^+$ moiety, thus favoring $\pi-\pi$ stacking and stabilization of cation−anion interactions.

Second, we wanted to incorporate light harvesting capability into these double salts with an eye to potential photoconductivity. This goal has been pursued by availing ourselves of the proven light-harvesting $[Pt(tpy)(CCPh)]^+$

cation,[26] which is an efficient chromophore in charge-transfer systems using a sacrificial donor and an acceptor.[27−35] Additionally, the $[Pt(tpy)(CCPh)]^+$ species has been shown to form metal−metal interactions with itself, making it a more attractive candidate for our metallophilic purposes.[36−38] The results of both innovations are reported herein.

In this work, we have developed a new family of double salts of the type $[Pt(tpy)X][Au(C_6F_5)_2]$ (X = Cl, **3**, Br, **4**, or I, **5**) by combining the $[Au(C_6F_5)_2]^-$ species with the $[Pt(tpy)X]^+$ moiety. Introducing a light-harvesting group into our new double salt family was achieved via substituting CCPh for a halide in the $[Pt(tpy)X]^+$ moiety to form $[Pt(tpy)(CCPh)[Au-(C_6F_5)_2]$, **6**.

Experimental Section

General Considerations. Dichloro(1, 5-cyclooctadiene)-platinum(II), phenylacetylene, and 2,2′:6′,2″-terpyridine were purchased from Sigma Aldrich Chemical Co. and used as received. Spectral grade acetonitrile (CH_3CN) was purchased from Fisher Scientific and distilled before use from CaH_2 under N_2. All other spectral grade reagents were used without further purification. $[Pt(tpy)Cl]Cl$,[39] $[Pt(tpy)I]I$,[15] $[Au(SC_4H_8)Cl]$,[40] and $[Bu_4N][Au(C_6F_5)_2]$[40] were prepared according to literature methods. The compound $[Pt(tpy)-Br]Br$[16] was prepared similarly to the iodide derivative.[15]

Characterization and Instrumentation. All mass spectra were collected using an Agilent 1100 LC/MSD with electrospray ionization (ESI) and atmospheric pressure chemical ionization (APCI) sources. Elemental analyses were performed by Quantitative Technologies Inc. (QTI, Whitehouse, NJ 08888). Absorption spectra were collected on a Shimadzu 3600 UV−vis−NIR spectrophotometer. Emission spectra were measured using an Jobin Yvon Horiba FluoroMax 3 fluorimeter.

X-ray Diffraction Studies. A summary of crystal data collection and refinement parameters for all compounds are given in Table 1. Selected interatomic distances and angles are given in Table 2. All data were collected on APEX-CCD-detector equipped Bruker diffractometers. Data for compound **5** were corrected for absorption using numerical methods, and all other structures were corrected for absorption using semiempirical, multiscan methods. All structures were solved by direct methods, and the remaining non-hydrogen atoms were located

(19) Hayoun, R.; Zhong, D. K.; Rheingold, A. L.; Doerrer, L. H. *Inorg. Chem.* **2006**, *45*, 6120.

(20) Uson, R.; Laguna, A.; Vicente, J. *J. Chem. Soc., Chem. Commun.* **1976**, 353.

(21) Uson, R.; Laguna, A.; Laguna, M.; Fernandez, E. *Inorg. Chim. Acta* **1980**, *45*, L177.

(22) Fernandez, E. J.; Laguna, A.; Olmos, M. E. *Coord. Chem. Rev.* **2008**, *252*, 1630.

(23) Fernandez, E. J.; Gimeno, M. C.; Laguna, A.; Lopez-de-Luzuriaga, J. M.; Monge, M.; Pyykkoe, P.; Sundholm, D. *J. Am. Chem. Soc.* **2000**, *122*, 7287.

(24) Fernandez, E. J.; Laguna, A.; Lopez-de-Luzuriaga, J. M.; Monge, M.; Montiel, M.; Olmos, M. E.; Rodriguez-Castillo, M. *Organometallics* **2006**, *25*, 3639.

(25) Fernandez, E. J.; Lopez-de-Luzuriaga, J. M.; Monge, M.; Montiel, M.; Olmos, M. E.; Perez, J.; Laguna, A.; Mendizabal, F.; Mohamed, A. A.; Fackler, J. P., Jr. *Inorg. Chem.* **2004**, *43*, 3573.

(26) Yam, V. W.-W.; Tang, R. P.-L.; Wong, K. M.-C.; Cheung, K.-K. *Organometallics* **2001**, *20*, 4476.

(27) Chakraborty, S.; Wadas, T. J.; Hester, H.; Flaschenreim, C.; Schmehl, R.; Eisenberg, R. *Inorg. Chem.* **2005**, *44*, 6284.

(28) Chakraborty, S.; Wadas, T. J.; Hester, H.; Schmehl, R.; Eisenberg, R. *Inorg. Chem.* **2005**, *44*, 6865.

(29) Du, P.; Knowles, K.; Eisenberg, R. *J. Am. Chem. Soc.* **2008**, *130*, 12576.

(30) Du, P.; Schneider, J.; Jarosz, P.; Eisenberg, R. *J. Am. Chem. Soc.* **2006**, *128*, 7726.

(31) Du, P.; Schneider, J.; Luo, G.; Brennessel, W. W.; Eisenberg, R. *Inorg. Chem.* **2009**, *48*, 4952.

(32) Yang, Q.; Wu, L.; Wu, Z.; Zhang, L.; Tung, C. *Inorg. Chem.* **2009**, *41*, 5653.

(33) Yang, Q.; Tong, Q.; Wu, L.; Wu, Z.; Zhang, L.; Tung, C. *Eur. J. Inorg. Chem.* **2004**, *2004*, 1948.

(34) Lu, W.; Mi, B.; Chan, M. C. W.; Hui, Z.; Che, C.; Zhu, N.; Lee, S. *J. Am. Chem. Soc.* **2004**, *126*, 4958.

(35) Du, P.; Schneider, J.; Jarosz, P.; Zhang, J.; Brennessel, W. W.; Eisenberg, R. *J. Phys. Chem. B* **2007**, *111*, 6887.

(36) Yam, V.; Tang, R. P.; Wong, K.; Cheung, K. *Organometallics* **2001**, *20*, 4476.

(37) Yu, C.; Wong, K.; Chan, K.; Yam, V. *Angew. Chem., Int. Ed.* **2005**, *44*, 791.

(38) Buechner, R.; Field, J. S.; Haines, R. J.; Ledwaba, L. P.; McGuire, R.; McMillin, D. R.; Munro, O. Q. *Inorg. Chim. Acta* **2007**, *360*, 1633.

(39) Annibale, G.; Pitteri, B.; Wilson, M. H.; McMillin, D. *Inorg. Synth.* **2004**, *34*, 76.

(40) Du, P.; Schneider, J.; Li, F.; Zhao, W.; Patel, U.; Castellano, F. N.; Eisenberg, R. *J. Am. Chem. Soc.* **2008**, *130*, 5056.

Table 1. Summary of X-ray Data Collection Parameters

	1	**2**	**3**	**4**	**5**	**6**
formula	$PtC_{15}N_3H_{15}Br_2O_2$	$Pt_2C_{49}N_7H_{41}F_{12}O_2P_2$	$PtAuC_{27}N_3H_{11}F_{10}Cl$	$PtAuC_{27}N_3H_{11}F_{10}Br$	$Pt_2Au_2C_{54}N_6H_{22}F_{20}I_2$	$PtAuC_{35}N_3H_{16}F_{10}$
FW	624.21	1440.01	994.89	1039.35	2172.69	1060.56
cryst syst	monoclinic	triclinic	monoclinic	monoclinic	monoclinic	monoclinic
space group	$P2(1)/n$	$P\bar{1}$	$P2(1)/c$	$P2(1)/c$	$P2(1)/n$	$P2(1)/n$
a, Å	6.9548(7)	13.1966(17)	22.6983(12)	22.7955(19)	14.4040(9)	16.7535(10)
b, Å	17.4240(18)	14.043(2)	6.7619(4)	7.7848(6)	24.4020(15)	7.5118(5)
c, Å	13.9923(14)	14.635(2)	16.6367(9)	16.6706(14)	15.0590(10)	23.6491(14)
α, deg	90	89.604(4)	90	90	90	90
β, deg	97.2600(10)	69.444(4)	100.1760(10)	100.128(2)	105.2240(11)	96.0760(10)
γ, deg	90	71.091(4)	90	90	90	90
V, Å^3	1682.0(3)	2384.8(6)	2513.3(2)	2538.1(4)	5107.3(6)	2959.5(3)
Z	4	2	4	4	4	4
ρ(calcd), g cm^{-3}	2.465	2.005	2.629	2.720	2.826	2.380
M(Mo Kα), mm^{-1}	13.105	6.024	11.597	12.953	12.519	9.770
T, K	100(2)	100(2)	100(2)	123(2)	150(2)	100(2)
R(F), %^{a}	3.81	5.99	3.02	2.22	7.99	3.62
R(wF^2), %^{b}	7.45	14.46	4.17	5.20	13.80	7.58

^{a} R $= \sum ||F_o| - |F_c|| / \sum |F_o|$. ^{b} R($wF^2$) $= \{\sum w(F_o^2 - F_c^2)^2 / \sum w(F_o^2)^2\}^{1/2}$; $w = 1/[\sigma^2(F_o^2) + (aP)^2 + bP]$, $P = [2F_c^2 + \max(F_o, 0)]/3$.

from subsequent difference maps. All structures were refined with anisotropic thermal parameters for all non-hydrogen atoms; hydrogen atoms were treated as idealized contributions. For compound **2** hydrogen atoms on water molecules were found from a Fourier difference map and although short H···H contacts were generated these hydrogen atoms were kept in the refinement. All software is contained in various libraries (SHELXTL, SMART, and SAINT) maintained by Bruker AXS, Madison, WI.[41]

Electronic Structure Calculations. Density functional theory (DFT) calculations used a QS8−2400C computer from Parallel Quantum Solutions (PQS) with the Amsterdam Density Functional Package 2008.01[42−44] on all-electron, geometry-optimized systems with TZ2P basis sets and the Vosko, Wilk, and Nusair[45] local density approximation, and scalar relativistic corrections. Calculations were carried out on six species with symmetry enforced as indicated: $[Pt(tpy)Cl]^+$ C_{2v}, $[Pt(tpy)(CCPh)]^+$ C_{2v}, $[AuCl_2]^-$ $D_{\infty h}$, $[AuCl(CN)]^-$ $C_{\infty v}$, $[Au(CN)_2]^-$ $D_{\infty h}$, and $[Au(C_6F_5)_2]^-$ D_{2h}. A comparison of intramolecular distances and angles from crystallographic studies with the computational data is presented in Supporting Information, Table S1. All structures were confirmed by frequency calculations which showed no negative frequencies.

Synthesis and Characterization

[Pt(tpy)Br]Br·2H$_2$O (1). The yellow product was isolated after the halide exchange reaction of [Pt(tpy)Cl]Cl with 5 equiv of KBr, as previously reported.[16] The yellow solid was recrystallized three times from a hot aqueous solution in 73.3% yield. Slow evaporation of a concentrated dimethylformamide (DMF) solution yielded yellow needles suitable for X-ray diffraction. The UV−vis spectrum has been reported previously.[46]

[Pt(tpy)(CCPh)]PF$_6$·$^1/_2$DMF·$^1/_2$H$_2$O (2). This compound was synthesized via a modification of the literature

method.[47] Triply recrystallized [Pt(tpy)Br]Br (102.8 mg, 0.176 mmol) was added to approximately 10 mL of DMF. Excess phenylacetylene (38.2 μL, 0.348 mmol) and triethylamine (200.4 μL, 1.438 mmol) were added to the suspension. The reaction flask was flushed with N$_2$, and a catalytic amount of CuI (4.0 mg, 0.0198 mmol) was added to the reaction. Upon addition of catalyst, the slurry turned red. The suspension was stirred under N$_2$ for 3 days. On the third day, an excess of KPF$_6$ (44.3 mg, 0.241 mmol) was added to the suspension and stirred for approximately 6 h. A green solid was precipitated from the suspension with the addition of water. The green solid was isolated via vacuum filtration and recrystallized from CH$_3$CN and Et$_2$O in 93.6% yield (80.3 mg). The UV−vis spectrum has been reported previously.[47]

[Pt(tpy)Cl][Au(C$_6$F$_5$)$_2$] (3). Solid [Bu$_4$N][Au(C$_6$F$_5$)$_2$] (103.7 mg, 0.100 mmol) was added to a stirred orange solution of [Pt(tpy)Cl]Cl (54.5 mg, 0.100 mmol) in a 5:1 CH$_3$CN/H$_2$O mix. A yellow precipitate formed immediately upon the addition. The resulting slurry was stirred for 12 h at room temperature. The yellow product was isolated via filtration, washed with three 5 mL portions of CH$_2$Cl$_2$, and recrystallized from hot CH$_3$CN to give a yellow microcrystalline solid (87.8 mg, 88% yield). Yellow needles suitable for X-ray diffraction were grown via evaporation of a dilute DMF solution. Anal. Calcd (%) for PtAuC$_{27}$H$_{11}$N$_3$F$_{10}$Cl: C, 32.60; H, 1.11; N, 4.22; F, 19.09. Found: C, 32.48; H, 1.27; N, 4.27; F, 19.02. ESI-MS: m/z (%) 462.9 (100) [M$^+$]; 530.7 (100) [M$^-$]. UV−vis (DMF) [λ_{max}, nm (ε, M^{-1} cm^{-1})]: 334 (13,100), 326 (9790), 351 (10,030), 379 (2380).

[Pt(tpy)Br][Au(C$_6$F$_5$)$_2$] (4). The yellow powder [Pt(tpy)-Br]Br (65.0 mg, 0.11 mmol) was dissolved in a 10:2:1 mixture of CH$_3$CN/DMSO/H$_2$O to form a yellow solution. Upon addition of an equimolar amount of [Bu$_4$N]-[Au(C$_6$F$_5$)$_2$] (114.0 mg, 0.11 mmol) to the solution, a yellow precipitate formed and was isolated via filtration. The yellow solid was obtained in 69.9% yield (56.2 mg) after washing with ether and recrystallization from hot CH$_3$CN to give yellow X-ray quality needles. Anal. Calcd (%) for PtAuC$_{27}$H$_{11}$N$_3$F$_{10}$Br: C, 31.20; H, 1.07; N, 4.04; F, 18.03. Found: C, 31.14; H, 0.97; N, 4.03; F, 18.33. ESI-MS: m/z (%) 508 (100) [M$^+$]; 531 (100) [M$^-$]. UV−vis

(41) Sheldrick, G. M. *Acta Crystallogr., Sect. A.* **2008**, *A64*, 112.
(42) Katz, M. J.; Sakai, K.; Leznoff, D. B. *Chem. Soc. Rev.* **2008**, *37*, 1884.
(43) Te Velde, G.; Bickelhaupt, F. M.; Baerends, E. J.; Fonseca Guerra, C.; Van Gisbergen, S. J. A.; Snijders, J. G.; Ziegler, T. *J. Comput. Chem.* **2001**, *22*, 931.
(44) Guerra, C. F.; Snijders, J. G.; Te Velde, G.; Baerends, E. J. *Theor. Chem. Acc.* **1998**, *99*, 391.
(45) Vosko, S. H.; Wilk, L.; Nusair, M. *Can. J. Phys.* **1980**, *58*, 1200.
(46) Yip, H.; Cheng, L.; Cheung, K.; Che, C. *J. Chem. Soc., Dalton Trans.* **1993**, *29*, 2933.
(47) Yang, Q.-Z.; Wu, L.-Z.; Wu, Z.-X.; Zhang, L.-P.; Tung, C.-H. *Inorg. Chem.* **2002**, *41*, 5653.

Table 2. Selected Interatomic Distances and Angles for Complexes **1−6**

complex	distances	(Å)	angles	(deg)
1	Pt(1)···Pt(1)	3.4674(4)	Pt(1)−Pt(1)−Pt(1)	126.94(1)
	Pt(1)···Pt(1)	4.2948(5)	N(2)−Pt(1)−Br(1)	178.27(15)
	Pt(1)−N(1)	2.029(5)	N(1)−Pt(1)−N(3)	162.2(2)
	Pt(1)−N(2)	1.931(5)		
	Pt(1)−N(3)	2.016(5)		
	Pt(1)−Br(1)	2.4218(7)		
2	Pt(1)···Pt(2)	3.3579(6)	N(1)−Pt(1)−N(3)	161.32(15)
	Pt(2)···Pt(2)	3.3632(6)	N(2)−Pt(1)−C(16)	178.5(3)
	Pt(1)−N(1)	2.013(6)	Pt(1)−C(16)−C(17)	177.0(7)
	Pt(1)−N(2)	1.980(6)	N(4)−Pt(2)−N(6)	161.6(2)
	Pt(1)−N(3)	2.015(6)	N(5)−Pt(2)−C(39)	179.1(3)
	Pt(1)−C(16)	1.982(8)	Pt(2)−C(39)−C(40)	178.5(7)
	C(16)−C(17)	1.187(11)		
	Pt(2)−N(4)	2.033(6)		
	Pt(2)−N(5)	1.957(6)		
	Pt(2)−N(6)	2.020(6)		
	Pt(2)−C(39)	2.978(7)		
	C(39)−C(40)	1.216(10)		
3	Pt(1)···Au(1)	4.7470(3)	N(2)−Pt(1)−Cl(1)	179.04(8)
	Au(1)···Pt(1)	4.091(2)	N(1)−Pt(1)−N(3)	162.43(12)
	Pt(1)−N(1)	2.017(3)	C(16)−Au(1)−C(22)	174.86(14)
	Pt(1)−N(2)	1.941(3)	Pt(1)−Au(1)−Pt(1)	99.58
	Pt(1)−N(3)	2.021(3)		
	Pt(1)-C(l1)	2.2977(9)		
	Au(1)−C(16)	2.039(3)		
	Au(1)−C(22)	2.045(3)		
4	Pt(1)···Au(1)	4.0574(3)	N(2)−Pt(1)−Br(1)	178.70(10)
	Au(1)···Pt(1)	4.7221(4)	N(3)−Pt(1)−N(1)	162.66(14)
	Pt(1)−N(1)	2.018(3)	C(1)−Au(1)−C(7)	174.78(16)
	Pt(1)−N(2)	1.940(4)	Pt(1)−Au(1)−Pt(1)	100.94
	Pt(1)−N(3)	2.017(4)		
	Pt(1)−Br(1)	2.4069(5)		
	Au(1)−C(1)	2.039(4)		
	Au(1)−C(7)	2.042(4)		
5	Pt(1)···Pt(2)	3.6817(8)	N(2)−Pt(1)−I(1)	179.7(4)
	Pt(1)···Pt(1)	3.6376(7)	N(1)−Pt(1)−N(3)	161.2(5)
	Pt(2)···Pt(2)	4.3046(9)	N(5)−Pt(2)−I(2)	177.9(3)
	Pt(1)−N(1)	2.031(12)	N(4)−Pt(2)−N(6)	162.0(5)
	Pt(1)−N(2)	1.932(12)	C(31)−Au(1)−C(37)	177.6(7)
	Pt(1)−N(3)	2.021(11)	C(43)−Au(2)−C(49)	178.4(6)
	Pt(1)−I(1)	2.5819(11)	Pt(2)−Pt(1)−Pt(1)	166.72(2)
	Pt(2)−N(4)	2.036(14)	Pt(2)−Pt(2)−Pt(1)	158.55(2)
	Pt(2)−N(5)	1.955(14)		
	Pt(2)−N(6)	1.991(14)		
	Pt(2)−I(2)	2.5706(13)		
	Au(1)−C(31)	2.060(15)		
	Au(1)−C(37)	2.074(15)		
	Au(2)−C(43)	2.040(16)		
	Au(2)−C(49)	2.055(15)		
6	Pt(1)···Pt(1)	3.3466(3)	N(1)−Pt(1)−N(3)	161.2(2)
	Pt(1)−N(1)	2.022(4)	N(2)−Pt(1)−C(16)	178.0(2)
	Pt(1)−N(2)	1.965(5)	Pt(1)−C(16)−C(17)	177.9(4)
	Pt(1)−N(3)	2.019(4)	C(24)−Au(1)−C(27)	175.8(5)
	Pt(1)−C(16)	1.991(5)	C(24)−Au(1)−C(24A)	179.56(3)
	C(16)−C(17)	1.179(6)	C(30)−Au(2)−C(33)	178.0(4)
	Au(1)−C(24)	2.101(6)	C(30)−Au(2)−C(30A)	177.97(7)
	Au(1)-C(24A)	2.121(5)		
	Au(2)−C(30)	2.109(5)		
	Au(2)-C(30A)	2.109(5)		

(DMF) [λ_{max}, nm (ε, M^{-1} cm^{-1})]: 335 (20,100), 353 (15,800), 382 (shoulder) (3260).

[Pt(tpy)I][Au(C$_6$F$_5$)$_2$] (5). Red [Pt(tpy)I]I (122.9 mg, 0.18 mmol) was dissolved in a 10:2:1 mixture of CH$_3$CN/DMF/H$_2$O to form an orange solution. Upon addition of equimolar [Bu$_4$N][Au(C$_6$F$_5$)$_2$] (187.0 mg, 0.18 mmol), a yellow precipitate formed and was isolated via filtration. After washing with ether, the yellow solid was

Scheme 1. Summary and Numbering Scheme of Compounds Used in This Study

1 X=Br, Y=Br	
2 X=CCPh, Y=PF$_6$	

3 X=Cl	
4 X=Br	
5 X=I	
6 X=CCPh	
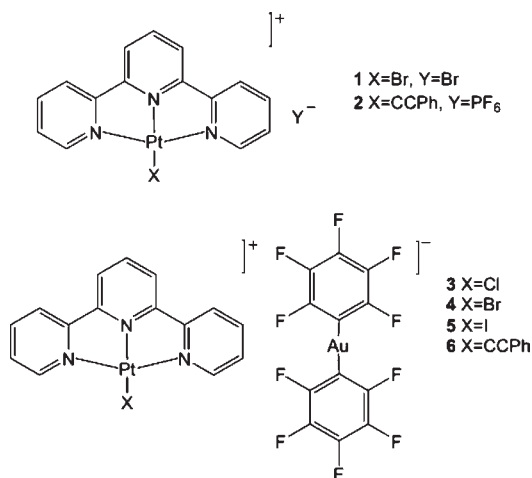
recrystallized from hot CH$_3$CN and isolated as orange needles suitable for X-ray diffraction in 69.9% yield (173.8 mg). Anal. Calcd (%) for PtAuC$_{27}$H$_{11}$N$_3$F$_{10}$I: C, 29.85; H, 1.02; N, 3.87; F, 17.49. Found: C, 29.98; H, 1.02; N, 3.82; F, 17.82. ESI-MS: m/z (%) 555 (100) [M$^+$]; 531 (100) [M$^-$]. UV−vis (DMF) [λ_{max}, nm (ε, M^{-1} cm^{-1})]: 331 (11,300), 349 (10,100), 427 (1850).
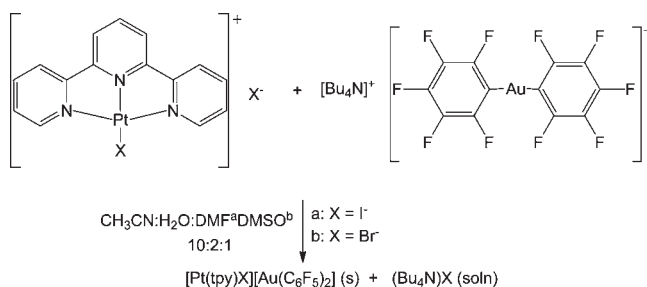
[Pt(tpy)(CCPh)][Au(C$_6$F$_5$)$_2$] (6). Solid [Bu$_4$N][Au(C$_6$F$_5$)$_2$] (113.1 mg, 0.109 mmol) was added to an orange solution of [Pt(tpy)(CCPh)](PF$_6$) (73.3 mg, 0.109 mmol) in 50 mL of CH$_3$CN. An orange precipitate formed after approximately 1 h. The resulting slurry was stirred for 12 h at room temperature and 100 mL of water were added to the slurry, resulting in precipitation of more orange solid. The orange product was isolated via filtration, washed with three 5 mL portions of CH$_2$Cl$_2$, and recrystallized via diffusion of ether into a DMF solution to form red crystals in 83% yield (100.0 mg). Anal. Calcd (%) for PtAuC$_{35}$H$_{16}$N$_3$F$_{10}$: C, 39.64; H, 1.52; N, 3.96; F, 17.91. Found: C, 39.91; H, 1.49; N, 4.02; F, 17.96. ESI-MS: m/z (%) 529.1 (100) [M$^+$]; 530.7 (100) [M$^-$]. UV−vis (DMF) [λ_{max}, nm (ε, M^{-1} cm^{-1})]: 316 (12,300), 333 (12,400), 347 (13,900), 440 (shoulder) (4870).

Results and Discussion

A summary of all the new compounds prepared and their numbering scheme is given in Scheme 1. Syntheses of these double salts used a general metathesis route similar to our previous synthetic methods, in which the double salt was precipitated and filtered away from the soluble byproduct.[7] Syntheses of the chloride and phenylacetylide derivatives were relatively straightforward while preparation of the bromide and iodide derivatives was more complicated because of [Pt(tpy)Cl]Cl impurities. To obtain better separation of products, the starting [Pt(tpy)X]X material for these derivatives was dissolved in an empirically determined solvent mixture as shown in Scheme 2.

Structural Characterization. Crystal data collection and refinement parameters for complexes **1−6** are presented in Table 1, and selected interatomic distances and angles are given in Table 2. The structure of complex **1** is similar to its parent complex, [Pt(tpy)Cl]Cl·2H$_2$O.[32] The asymmetric unit contains one [Pt(tpy)Br]$^+$ moiety and one bromide atom with two water molecules. As shown in
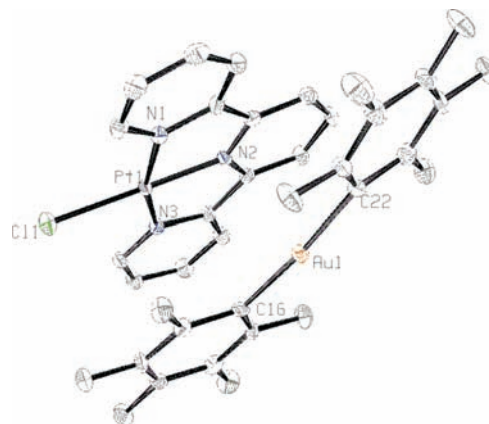
Scheme 2. Synthesis of $[Pt(tpy)X][Au(C_6F_5)_2]$ for $X = Br^-$ (**4**) and I^- (**5**)

Figure 1. ORTEP of $[Pt(tpy)Cl][Au(C_6F_5)_2]$ (**3**) with 50% displacement ellipsoids. Hydrogen atoms removed for clarity.

Supporting Information, Figure S1, the platinum is co-ordinated to three nitrogen atoms from the terpyridine ligand with the fourth site occupied by a bromide atom. The platinum center sits in a distorted square planar environment with an $N(2)-Pt(1)-Br(1)$ angle of 178.27(15)°. Like $[Pt(tpy)Cl]Cl \cdot H_2O$, complex **1** forms close pairwise head-to-tail cation interactions with a short $Pt \cdots Pt$ distance of 3.4674(4) Å, followed by a long contact with its neighbor at a distance of 4.2948(5) Å. The pairwise $Pt \cdots Pt$ distance in this structure is slightly longer than that observed in the previously reported $[Pt(tpy)Br][AuBr_2]$ complex.[48] These pairwise interactions extend in one direction to form an array of cations (Supporting Information, Figure S2). The spaces between the cation arrays are filled in by water molecules and bromide counterions. As shown in Supporting Information, Figure S2, each bromide ion sits between pairs of water molecules, which span 5.397(8) Å from $O(1)-Br(2)$ (Supporting Information, Figure S2) and fill in the space between the long $Pt \cdots Pt$ contacts. The $Br(2)-H(1A)$ distance of 3.5(1) Å between the pairwise interactions is much shorter (Supporting Information, Figure S2). The $[Pt(tpy)Br]^+$ cation has been shown previously[16] to participate in infinite chains of metallophilic interactions.

The structure of complex **2** is unremarkable and similar to that reported in the literature (Supporting Information, Figure S3).[36] The cations stack in a head-to-tail fashion, forming a zigzag extended chain with two distinct $Pt \cdots Pt$ distances of 3.3579(6) and 3.3632(6) Å (Supporting Information, Figure S3). The empty spaces between the cation chains are filled in by both solvent (DMF, H_2O) and counteranion (PF_6^-) species. This solvated structure demonstrates the crystal packing sensitivity to solvent conditions, with different recrystallization methods yielding different colored crystals that have distinct $Pt \cdots Pt$ distances between $[Pt(tpy)(CCPh)]^+$ cations. For example, the CH_3CN solvate of $[Pt(tpy)(CCPh)]PF_6$ is dark purple and has two unique $Pt \cdots Pt$ contacts of 3.3747(9) and 3.3626(9) Å.[26] In the $[Pt(tpy)Cl]Cl$ case, the water solvate is yellow with pairwise $Pt \cdots Pt$ contacts, whereas the dimethylsulfoxide (DMSO) solvate is red with infinite chains of $Pt \cdots Pt$ metallophilic interactions.[6]

The asymmetric unit of complex **3** is shown in Figure 1 with one cation and one anion. In the cation, three nitrogen atoms of the terpyridine ligand occupy three coordination sites of the Pt^{II} center, and the chloride

occupies the fourth coordination site. The Pt^{II} center sits in a distorted square planar environment with an $N(2)-Pt(1)-Cl(1)$ angle of 179.04(8)°. In the anion, the Au^I center sits in a near linear environment between two aryl groups with a $C(16)-Au(1)-C(22)$ angle of 174.86(14)°.

Despite the low steric bulk above and below the molecular plane in both the cation and the anion, the $Pt \cdots Au$ distances are significantly larger than the sum of the van der Waals radii of the two metals (3.41 Å).[49] A closer look at the structure, as shown in Figure 2, reveals that the shortest contacts between the two species occurs between $Pt(1)$ of the cation and $C(21)$ of the anion, with alternating distances of 3.405(3) and 3.399(3) Å. The terpyridine group of the cation sits directly on top of the aryl group of the anion, resulting in long $Pt \cdots Au$ distances (4.0901(2) and 4.7470(3) Å). It appears that electrostatic attraction between the $Pt(\delta^+)$ and $C_{ortho}(\delta^-)$ dominates the crystal packing forces, shifting the gold atom of the anion to the side of the platinum atom, resulting in a zigzag pattern with $Pt \cdots Au$ distances outside of the sum of the van der Waals radii for the two atoms. The packing of the complexes also exhibits π-stacking between C_6F_5 groups on adjacent anions (Supporting Information, Figure S4). As shown in Supporting Information, Figure S4, one-dimensional arrays of cations and anions line up parallel to one another with two sets of interacting aryl groups on either side.

The structure of complex **4** is similar to that of complex **3** and is shown in Supporting Information, Figure S5. The asymmetric unit contains one cation and one anion. The Pt^{II} center sits in a distorted square planar environment with an $N(2)-Pt(1)-Br(1)$ angle of 178.79(10)°. In the anion, the Au^I atom exhibits near linear coordination with a $C(1)-Au(1)-C(7)$ angle of 174.78(16)°. As shown in Supporting Information, Figure S6, the stacking pattern of the complex **4** is nearly identical to complex **3**, with the terpyridine group of the cation sitting directly on top of the aryl group of the anion. Again, the closest contact between the two moieties is between $Pt(1)$ and $C(2)$ (3.387(4) and 3.435(5) Å), with the gold atom shifted relative to the platinum atom, resulting in long $Pt \cdots Au$

(48) Schneider, J.; Du, P.; Jarosz, P.; Lazarides, T.; Wang, X.; Brennessel, W. W.; Eisenberg, R. *Inorg. Chem.* **2009**, *48*, 4306.

(49) Jarosz, P.; Thall, J.; Schneider, J.; Kumaresan, D.; Schmehl, R.; Eisenberg, R. *Energy Environ. Sci.* **2008**, *1*, 573.
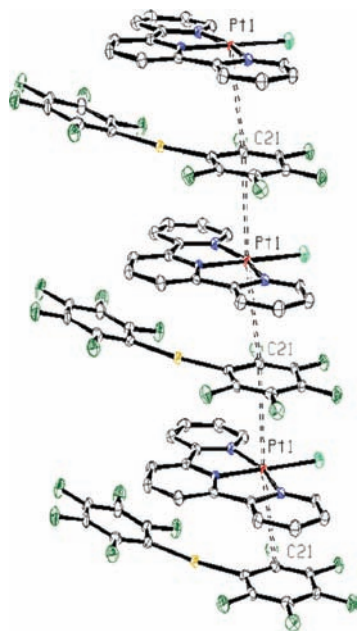
Figure 2. Extended stacking of [Pt(tpy)Cl][Au(C_6F_5)$_2$] (**3**) showing close contacts between Pt(1) of the cation and C(21) of the anion with two crystallographically independent Pt···C distances of 3.399(3) (C(21)−Pt(1)) and 3.405(3) (Pt(1)−C(21)) Å. Hydrogen atoms removed for clarity.
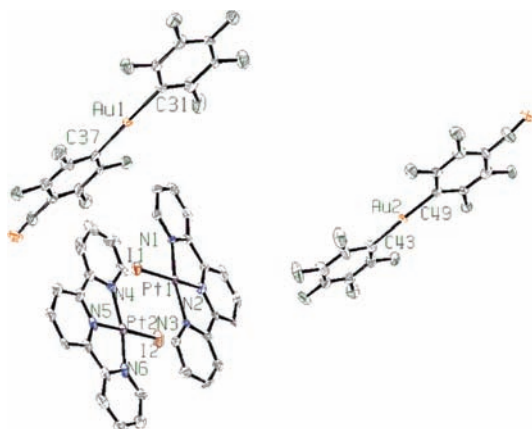
Figure 3. ORTEP of [Pt(tpy)I][Au(C_6F_5)$_2$] (**5**) with 50% displacement ellipsoids. Hydrogen atoms removed for clarity.

distances of 4.057(3) and 4.7221(4) Å. Similar to the packing of complex **3**, the aryl groups from adjacent anions interact with each other, further stabilizing the infinite chain of atoms (Supporting Information, Figure S7). Unlike the recently reported [Pt(tpy)Br][AuBr$_2$] structure,[16] this [Pt(tpy)Br][AuX$_2$] double salt does not display Pt···Au interactions, but only interactions between the platinum centers and the ortho-carbon of the aryl ring.

The structure of complex **5**, [Pt(tpy)I][Au(C_6F_5)$_2$], is shown in Figure 3 with important distances and angles listed in Table 2. The asymmetric unit contains two cations and two anions. Similar to the Pt^{II} environment reported for [Pt(tpy)I][AuI$_2$], the Pt^{II} center of the cation is coordinated by the three imine groups of the terpyridine ligand with the fourth coordination site occupied by iodide in a distorted square planar environment with an N(3)−Pt(1)−N(1) angle of 161.2(5)°.[15] The Au^{I} center of the anion rests in an almost linear environment with an C(43)−Au(2)−C(49) angle of 178.4(6)°.
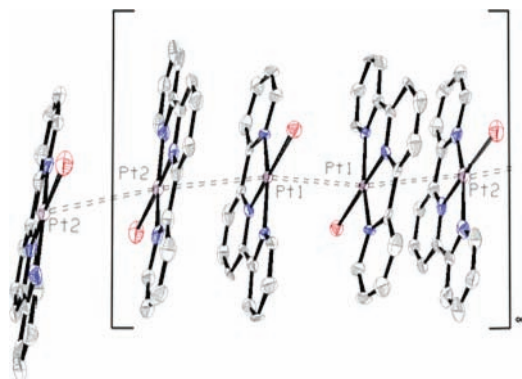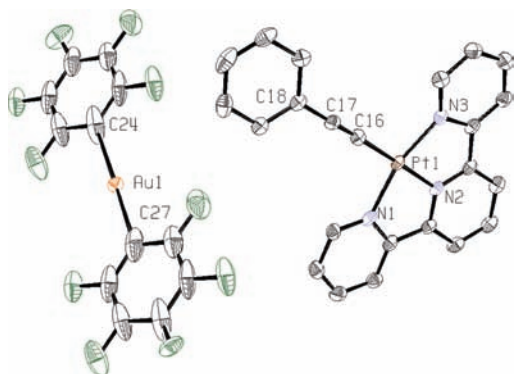

Figure 4. Infinite chain of [Pt(tpy)I]$^+$ moieties in [Pt(tpy)I][Au(C_6F_5)$_2$] (**5**) formed between Pt(2)···Pt(2), Pt(2)···Pt(1), and Pt(1)···Pt(1) contacts with the distances of unique Pt···Pt distances of 3.6817(8), 3.6376(7), and 4.3046(9) Å, respectively. Counter [Au(C_6F_5)$_2$]$^−$ anions and hydrogen atoms removed for clarity.

Unlike complexes **3** and **4**, the cations and anions in complex **5** do not stack in an alternating fashion. Instead, the cations form an infinite zigzag array defined by three unique Pt···Pt distances of 3.6817(8) (Pt(1)−Pt(2)), 3.6376(7) (Pt(1)−Pt(1)), and 4.3046(9) (Pt(2)−Pt(2)) Å as shown in Figure 4. The first two internuclear distances between Pt(1)−Pt(2) and Pt(1)−Pt(1) are near the sum of the van der Waals radii for the two metal centers, and therefore could be considered a metallophilic interaction. The zigzag chain of [Pt(tpy)I]$^+$ moieties is characterized by two angles of 158.55(2)° (Pt(1)−Pt(1)−Pt(2)) and 166.72(2)° (Pt(2)−Pt(2)−Pt(1)). This tetracationic unit, Pt(1)−Pt(2)−Pt(2)−Pt(1), is repeated in one direction, forming an infinite series of cations. The anions in the structure stack in a slipped head-to-tail fashion, supported within by mutual π-interactions of the perfluoroaryl groups, and sandwich the cation chain (Supporting Information, Figure S8), with a position disorder of 92/8% for Au1/Au1B and 90/10% for Au2/Au2B.

The structure of complex **6** contains one [Pt(tpy)-(CCPh)]$^+$ moiety and a disordered [Au(C_6F_5)$_2$]$^−$ moiety (Figures 5 and Supporting Information, Figure S9) in which the [Au(C_6F_5)$_2$]$^−$ anions exhibit a disorder with interwoven or overlapping structures where the Au and para-F atoms can be thought of as alternating positions. This problem was treated by generating the second half of each [Au(C_6F_5)$_2$]$^−$ anion and then setting the occupancies to 50%. This resulted in long Au(1)−C(24), Au(1)−C(24A) distances of 2.101(6) and 2.121(5) and for Au(2)−C(30), Au(2)−C(30A) distances of 2.109(5), 2.109(5) Å compared to 2.04−2.05 Au−C values in compound **5**.

The crystal packing of complex **6** is similar to that of complex **5**, with the cations forming a channel supported by close pairwise Pt···Pt contacts insulated by slipped-head-to-tail anions on either side (Figure 6). The geometry about the metal centers in both the cation and the anion are similar to those of the starting materials. As shown in Figure 6, the cations form a zigzag pattern with Pt···Pt distances of 3.3466(3) and 4.3703(4) Å. These two distances define the tricationic unit, Pt(1A)−Pt-(1B)−Pt(1A), that is repeated in one direction. Just as in complex **5**, the anions do not participate in metal−metal interactions in this structure.
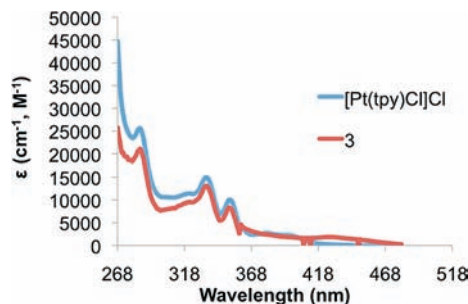
Figure 5. ORTEP of [Pt(tpy)(CCPh)][Au(C$_6$F$_5$)$_2$] (**6**) with 50% displacement ellipsoids. Hydrogen atoms removed for clarity.
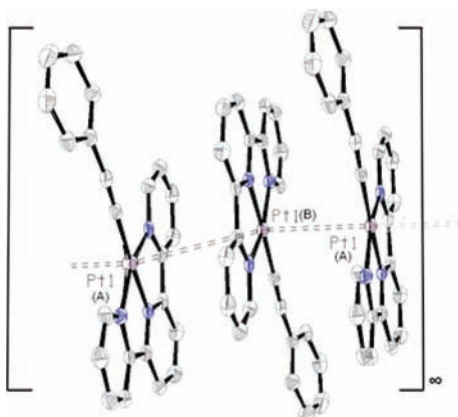
Figure 6. Infinite chain of [Pt(tpy)(CCPh)]$^+$ moieties in [Pt(tpy)-(CCPh)][Au(C$_6$F$_5$)$_2$] (**6**) with Pt···Pt contacts shown with dashed lines with an intradimer Pt(1(A))−Pt(1(B)) distance of 3.3466(3) Å and an interdimer Pt(1(B))−Pt(1(A)) distance of 4.3703(4) Å. Counter [Au(C$_6$F$_5$)$_2$]$^-$ anions and hydrogen atoms removed for clarity.

Absorption Spectra. The room temperature absorption spectra of all complexes were collected in DMF. The absorption spectra for the double salt complexes **3**, **4**, **5**, and **6** are shown in the Supporting Information, Figure S10. The solution spectra of the double salt complexes do not differ from the spectra of the [Pt(tpy)X]$^+$ starting complexes. The UV−vis spectra of complexes [Pt(tpy)Cl]-[Au(C$_6$F$_5$)$_2$], **3**, and [Pt(tpy)Cl]Cl are presented in Figure 7 and demonstrate that the Pt starting material and double salt spectra are effectively identical in solution. Therefore, the observed transitions are localized on the cations with neglible anion interaction, indicating that the cation and anion of the double salt do not interact in solution at these concentrations.

Absorptions at high energies (< 350 nm) with molar absorptivities on the order of 10^4 M^{-1} cm^{-1} are assigned to intraligand charge transfer (ILCT) of the cation's terpyridine ligand.[50] The less intense absorptions at lower energies (> 400 nm) with molar absorptivities on the order of 10^3 M^{-1} cm^{-1} are assigned to the ^{3}MLCT (metal-to-ligand charge transfer) transitions, which are attributed to the d(Pt)→ π*(tpy) transition.[50] As seen in previous systems, the lower energy transitions are dependent on the

(50) McMillin, D. R.; Moore, J. J. *Coord. Chem. Rev.* **2002**, *229*, 113.
(51) Aldridge, T. K.; Stacy, E. M.; McMillin, D. R. *Inorg. Chem.* **1994**, *33*, 722.

**Figure 7.** Absorption spectra of [Pt(tpy)Cl]Cl and [Pt(tpy)Cl][Au-(C$_6$F$_5$)$_2$], **3**.

nature of the X ligand coordinated to the Pt^{II} center.[51] The more electron donating the ligand, the lower the energy of this transition because of an increase in the metal-based highest occupied molecular orbital (HOMO) energy, which results in a smaller energy gap between the d$_z$(Pt) and π*(tpy) orbitals responsible for the transition.[51] As predicted, the absorption of complex **6** is red-shifted relative to that of the halides because of the electron donating phenylacetylide group. The absorption profiles of complexes **3** and **6** are shown in Supporting Information, Figure S10 and clearly show this red shift of approximately 40 nm in the visible range from roughly 420 nm (**3**) to roughly 460 nm (**6**).

Emission Spectra. In luminescent compounds, the energy and intensity of emission are generally governed by (1) the energy gap between the HOMO (donor) and lowest unoccupied molecular orbital (LUMO, acceptor) orbitals, (2) the degree of orbital overlap, (3) reorganization of the excited state, and (4) the average displacement of the transferred electron.[33] For [Pt(tpy)X]$^+$ systems, the HOMO is generally the d$_{z^2}$ orbital of the Pt^{II} center.[33] Previous studies of [Pt(tpy)X]$^+$ salts have shown some of these species to be emissive at room temperature in acetonitrile and acetonitrile/water solutions.[50,51] The [Pt(tpy)Cl]$^+$ systems are non-emissive at room temperature, but when cooled to 77 K, these chloride complexes are weakly emissive with only one excited state observed.[50] Luminescence has been attributed to excitation of a metal-based d$_{z^2}$ orbital (HOMO) electron of the metal center into a ligand based LUMO.[50] For systems where X is CCPh, room temperature emission is observed and tends to be more intense with a longer lived excited-state.[28] The increased emission intensity and stability of the excited-state is attributed to a decrease in the HOMO−LUMO gap because of an increase of the energy of the metal-based HOMO from the σ-donation of the phenylacetylide into the metal d$_{z^2}$ orbital. For the same complex, a red shift in the emission is observed when measured in the solid-state.[26] This excitation has been assigned to a triplet-state metal-to-metal-to-ligand charge transfer (^{3}MMLCT), which arises from significant Pt···Pt interactions in the solid.[26]

In this study, all [Pt(tpy)X][Au(C$_6$F$_5$)$_2$] complexes where X is a halide are non-emissive at room temperature in DMF. We did not anticipate the cation or the anion to be independently luminescent at room temperature. As described above, the halides are not sufficiently electron-donating to raise the energy of the HOMO of the molecule. Therefore, the HOMO−LUMO gap is too large of an energetic barrier. For the double salt systems, however, we
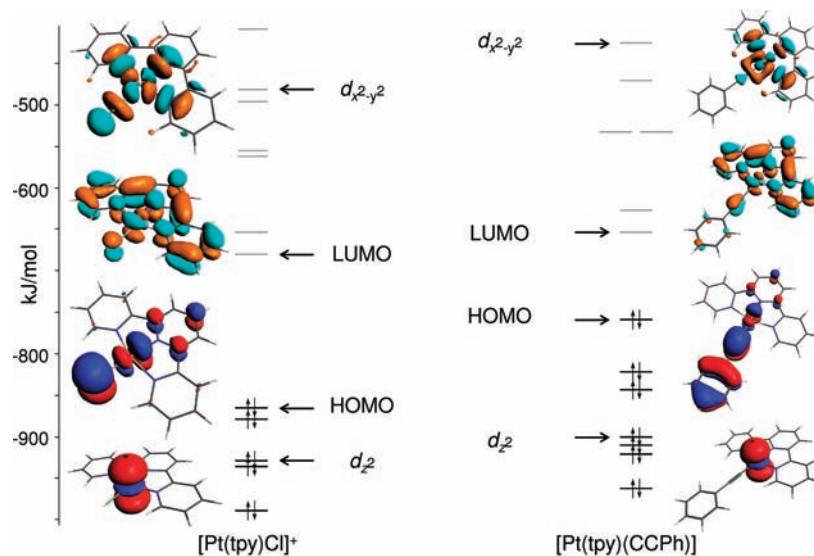
Figure 8. Molecular orbital (MO) calculations for $[Pt(tpy)Cl]^+$ (left) and $[Pt(tpy)(CCPh)]^+$ (right). Occupied orbitals are shown with black lines and red/blue electron density pictures. Unoccupied orbitals are shown with gray lines and orange/turquoise pictures. For each cation, only four orbitals (two occupied and two unoccupied) are explicitly depicted, and the levels to which they correspond are shown with arrows.

hypothesized that the LUMO of the $[Au(C_6F_5)_2]^-$ moiety would be closer in energy to the HOMO of the $[Pt(tpy)X]^+$ cation than in the $[Pt(tpy)X]^+X^-$ salts, thus providing a smaller energy gap for electron excitation. However, the lack of luminescence of the double salt complexes suggests that such a transition does not occur in solution under these conditions. The room temperature, solution state emission of complex **6** in DMF does not differ from that of complex **2**, which indicates that luminescence is attributed to the $[Pt(tpy)(CCPh)]^+$ species with no participation of the anion in the double salt.

Electronic Structure Calculations. As described above, complexes **3** and **4** display relatively long Pt···Au distances, while complexes **5** and **6** form varying degrees of Pt···Pt interactions with no Pt···Au interactions observed in the solid state. Surprisingly, the $[Pt(tpy)X]$-$[Au(C_6F_5)_2]$ double salts in this study do not behave like our previously reported $[Pt(tpy)Cl][Au(CN)_2]$ or $[Pt(tpy)$-$CN][AuCl(CN)]$ double salts[19] in the solid state, which form infinite chains of Pt···Au species defined by close metal−metal contacts. There is no obvious steric reason why the Pt and Au atoms cannot be in closer contact. Therefore, in an attempt to understand the differences between these earlier complexes and these new complexes that exhibit long Pt···Au distances, and some short Pt···Pt distances, we must consider both the steric and the electronic differences among these $[Pt]^+[Au]^-$ double salts. Considering first the steric properties of the new complexes, the primary effect is that the extension of the X group above and below the xy plane changes, increasing in the following order: **3** ∼ **6** < **4** < **5**. The greater spatial extension of the CCPh group into the xy plane is not believed to have a steric impact on the stacking, although an electronic impact from $\pi−\pi$ stacking cannot be excluded. To a first approximation, one would expect that the complexes with the smaller X groups would form closer metal−metal distances; however, this is not borne out by the structural data in the absence of crystallization solvent. (In the related $[Pt(tpy)X][AuX_2]$ system, the Br derivative exhibits shorter Pt···Au distances than the chloride.[17])

Therefore, electronic factors must also play a role in determining solid-state interactions within this family of compounds. An investigation with DFT was undertaken in an effort to elucidate any of these electronic influences.

Our initial picture of metallophilic interactions in terms of molecular orbitals involved a nucleophilic, metal-based HOMO of the anion donating into an electrophilic metal-based LUMO of the cation. In such an analysis, the relative energy, symmetry, and composition of the HOMO and LUMO of the moieties in question are potentially relevant in the formation of metallophilic interactions. Therefore, it is useful to inspect the MO diagrams of the building blocks of our compounds. We note that state-of-the-art computational work on noncovalent M···M interactions has demonstrated the important role of dispersion and correlation effects.[52−54] These effects are not currently accurately accounted for in commercial DFT programs and are furthermore not accessible to chemical intuition for those who, like us, wish to use that intuition in molecular design. The calculations discussed herein are intended to provide testable hypotheses for this intuition.

Figure 8 shows an energy level diagram comparison between $[Pt(tpy)Cl]^+$ and $[Pt(tpy)(CCPh)]^+$, with only the four orbitals under discussion depicted explicitly. In each cation, the HOMO is largely based on the X group, namely, the π-donating Cl in the first case and the π-accepting CCPh in the second. The LUMO is also similar between both compounds and is dominated by the terpyridine ligand. We anticipated that the stronger σ-donor character of CCPh versus Cl would raise the energy of the d_{z^2} orbital relative to the other occupied frontier orbitals in the compound and thereby promote metallophilic interactions between the Pt^{II} center of the cation and the Au^I center of the anion. This is clearly not the case as the HOMO in the CCPh cation is higher

(52) Grimme, S.; Djukic, J.-P. *Inorg. Chem.* **2010**, *49*, 2911.
(53) Schwabe, T.; Grimme, S.; Djukic, J.-P. *J. Am. Chem. Soc.* **2009**, *131*, 14156.
(54) Hyla-Kryspin, I.; Grimme, S.; Djukic, J.-P. *Organometallics* **2009**, *28*, 1001.
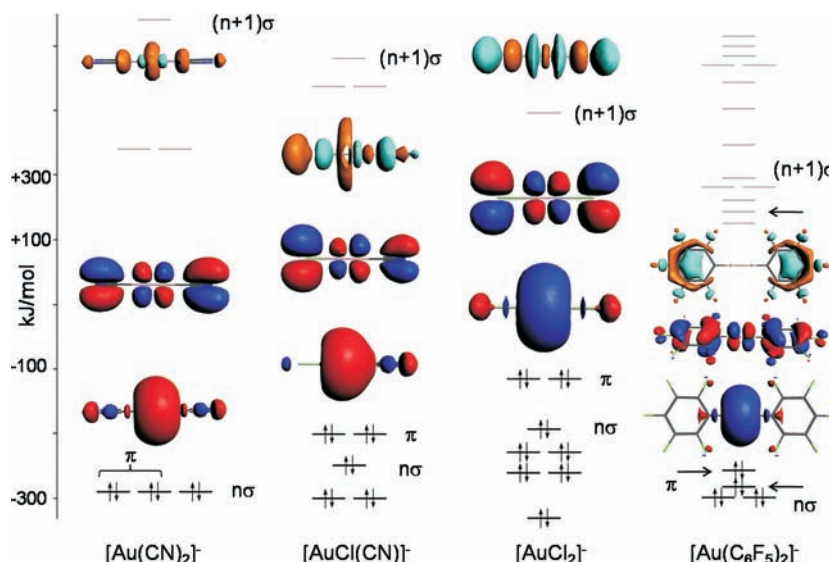
Figure 9. From left to right, molecular orbital (MO) calculations for $[Au(CN)_2]^-$, $[Au(CN)Cl]^-$, $[AuCl_2]^-$, and $[Au(C_6F_5)_2]^-$. Occupied orbitals are shown with black lines and red/blue electron density pictures. Unoccupied orbitals are shown with gray lines and orange/turquoise pictures. For each anion, three orbitals are depicted (from bottom to top) $n\sigma$, π, and $(n+1)\sigma$. The appropriate labels are placed next to the energy levels to which they correspond.

relative to the d_{z^2} than in the Cl instance, although Pt···Pt interactions are observed in **6**.

A similar comparison is presented in Figure 9 in which four different $[AuX_2]^-$ anions are shown. In previous work, we have established that $[Au(CN)_2]^-$ and $[AuCl(CN)]^-$ form infinite chains of metallophilic interactions in $[Pt]^+[Au]^-$ double salts.[19] With the same $[Pt(tpy)Cl]^+$ cation, however, the $[AuCl_2]^-$ anion forms only half as many metallophilic interactions. In the current work, $[Au(C_6F_5)_2]^-$ has formed no such close Pt···Au contacts with any $[Pt(tpy)X]^+$ cation to date. For each anion, three orbitals from each energy level diagram are labeled and depicted: the highest occupied π-type orbital, the highest occupied σ-type (labeled $n\sigma$), and lowest unoccupied σ-type orbital (labeled $(n+1)\sigma$). As for all bonding interactions, the correct symmetry is a sine qua non. Metallophilic interactions can involve a σ-type overlap between metal centers,[3,55] and in the linear geometry of $[AuX_2]^-$ anions, the orbital that can interact metallophilically must do so approximately perpendicular to the X-Au-X line. All four anions have such an orbital available, but only in the $[Au(CN)_2]^-$ case is this orbital (effectively) the HOMO. In the other three cases, the highest lying π-type orbital is higher in energy that the σ-type, which may reduce its propensity for metallophilic interactions. Significantly, the HOMO in $[Au(C_6F_5)_2]^-$ has substantial electron density on the *ortho* carbon atoms, which interact strongly with Pt in **3** and **4**. Also important in metallophilicity is an unoccupied σ-type orbital. In the first three anions, the lowest σ-type orbital (not necessarily the LUMO) has substantial metal character. However, this is not the case in $[Au(C_6F_5)_2]^-$, where again the $(n+1)\sigma$ orbital is dominated by the perfluoroaryl ring.

Thus, the DFT computational analysis reveals two delicate electronic forces that are both in play: metallophilic interactions and interactions of the C_6F_5 aryl ring with either $[PtL_3X]^+$ cations or itself. In complexes **3** and

4, we see strong interactions between the electron rich aryl group of the anion and the electron rich platinum centers of the cation, resulting in cation–anion stacking, with the closest contact being between the *ortho* carbon and the platinum center. In complexes **5** and **6**, however, the closest contact occurs between two relatively electron rich platinum centers of the cations, resulting in a cation–cation stacking pattern. The computational analysis suggests that the $[Au(C_6F_5)_2]^-$ is not suited to form metallophilic interactions with a $[PtL_3X]^+$ cation because its σ-type frontier orbitals are not localized strongly enough on the Au atom. This anion has been shown to form many metallophilic interactions with Ag[24,56–59] and Tl,[14,57,60–63] whose σ-donor orbitals for metallophilicity are not so strongly directional as in $[Pt(tpy)X]^+$.

It is also true that the four different $[Pt(tpy)X]^+$ cations studied here have different electron densities on the Pt atoms, which can influence whether or not these cations interact with each other when they do not do so with an anion. The most electron rich center is in the cation of **6**, and its crystal structure shows the shortest metallophilic contacts within this series. The cation of **5** has previously been shown to form only very long Pt···Pt contacts with itself,[16] which phenomenon is attributed to the significant

(55) Roundhill, D. M.; Gray, H. B.; Che, C. M. *Acc. Chem. Res.* **1989,** *22,* 55.

(56) Uson, R.; Laguna, A.; Laguna, M.; Jones, P. G.; Sheldrick, G. M. *J. Chem. Soc., Chem. Commun.* **1981,** 1097.

(57) Uson, R.; Laguna, A.; Laguna, M.; Manzano, B. R.; Jones, P. G.; Sheldrick, G. M. *J. Chem. Soc., Dalton Trans.* **1984,** 285.

(58) Fernandez, E. J.; Gimeno, M. C.; Laguna, A.; Lopez-de-Luzuriaga, J. M.; Monge, M.; Pyykkoe, P.; Sundholm, D. *J. Am. Chem. Soc.* **2000,** *122,* 7287.

(59) Fernandez, E. J.; Lopez-de-Luzuriaga, J. M.; Monge, M.; Olmos, M. E.; Puelles, R. C.; Laguna, A.; Mohamed, A. A.; Fackler, J. P., Jr. *Inorg. Chem.* **2008,** *47,* 8069.

(60) Fernandez, E. J.; Jones, P. G.; Laguna, A.; Lopez-de-Luzuriaga, J. M.; Monge, M.; Perez, J.; Olmos, M. E. *Inorg. Chem.* **2002,** *41,* 1056.

(61) Fernandez, E. J.; Jones, P. G.; Laguna, A.; Lopez-de-Luzuriaga, J. M.; Monge, M.; Montiel, M.; Olmos, M. E.; Perez, J. *Z. Naturforsch., B: Chem. Sci.* **2004,** *59,* 1379.

(62) Fernandez, E. J.; Laguna, A.; Lopez-de-Luzuriaga, J. M.; Montiel, M.; Olmos, M. E.; Perez, J. *Inorg. Chim. Acta* **2005,** *358,* 4293.

(63) Fernandez, E. J.; Laguna, A.; Lopez-de-Luzuriaga, J. M.; Montiel, M.; Olmos, M. E.; Perez, J. *Organometallics* **2006,** *25,* 1689.

steric bulk of iodide. The $[Pt(tpy)Cl]^+$ and $[Pt(tpy)Br]^+$ cations have exhibited metallophilic interactions with themselves,[6,15,16] and therefore the stacking in **3** and **4** is attributed to both the electrostatic attraction between cation and anion as well as the localization of HOMO electron density in $[Au(C_6F_5)_2]^-$ on the aryl rings, as shown in Figure 9.

Conclusions

In summary, we have synthesized and characterized four new double salt complexes of the type $[Pt(tpy)X][Au(C_6F_5)_2]$ (X = Cl, **3**, Br, **4**, I, **5**, CCPh, **6**, as well as crystallographically characterized two $[Pt(tpy)X]Y$ starting materials (X = Y = Br, **1**, and X = CCPh, Y = PF_6, **2**). Structural characterization shows that these double salt complexes form two types of structural motifs in the solid state. Complexes **3** and **4** form chains of alternating cation−anion moieties with long $Pt \cdots$ Au distances that lie well outside of the range of metallophilic interactions. Complexes **5** and **6** form cation stacks in channels characterized by pairwise $Pt \cdots Pt$ contacts in **6** and longer, barely metallophilic contacts in **5** with slipped-head-to-tail anions surrounding the cation chains. Significant metallophilic cation−anion interactions are absent in both packing patterns. Solution spectra (UV−vis and fluorescence) of these double salt complexes are nearly identical to their parent $[Pt(tpy)X]^+$ complexes, indicating the absence of

cation−anion interaction in the solution state. We believe that the lack of $Pt \cdots Au$ interactions is due to the ligand-based HOMO and LUMO on the $[Au(C_6F_5)_2]^-$ moiety as revealed via electronic structure calculations, which do not have orbitals of σ symmetry at the right energy to favorably overlap with the directional d_{z^2} orbital of the $[Pt]^+$ cations. As a result, the interactions in the double salt are observed to be either $Pt \cdots C$ *ortho* or $Pt \cdots Pt$ interactions in the solid state. We are cognizant of the possibility for alternative stacking formations in the presence of crystallization solvent. Future exploration of our double salt systems will investigate alternative $[AuX_2]^-$ anions that have greater electron density located in σ symmetry frontier orbitals of Au so as to favor direct $M \cdots M$ contacts.

Supporting Information Available: CIFs are given for compounds **1**−**6** as well as additional figures for aryl group interactions in complexes **3** and **4** (Figures S7 and S6), ORTEPs of complexes **1**, **4**, and **2** (Figures S1, S6, and S8), crystal packing diagrams for **1**, **4**, **5**, and **6** (Figures S2, S6, and S7, S9), as well as UV−vis spectra of **3**, **4**, **5**, and **6** in S10. This material is available free of charge via the Internet at http://pubs.acs.org.